Structural Engineering and Mechanics, *Vol. 70, No. 6 (2019) 661-669*
DOI: https://doi.org/10.12989/sem.2019.70.6.661

Semi-analytical solution for buckling of SMA thin plates with linearly distributed loads

Fatemeh Salemizadeh Parizi[a] and Meisam Mohammadi*

Department of Mechanical Engineering, Vali-e-Asr University of Rafsanjan, Rafsanjan, Iran

(Received December 6, 2018, Revised March 9, 2019, Accepted March 16, 2019)

Abstract. Buckling analysis of shape memory alloy (SMA) rectangular plates subjected to uniform and linearly distributed in-plane loads is the main objective in the present paper. Brinson's model is developed to express the constitutive characteristics of SMA plate. Using the classical plate theory and variational approach, stability equations are derived. In addition to external in-plane mechanical loads, the plate is subjected to the pre-stresses caused by the recovery stresses that are generated during martensitic phase transformation. Ritz method is used for solving the governing stability equations. Finally, the effects of conditions on the edges, thickness, aspect ratio, temperature and pre-strains on the critical buckling loads of SMA plate are investigated in details.

Keywords: shape memory alloy; Brinson's model; buckling analysis; Ritz method; classical plate theory

1. Introduction

Todays, plates are widely used in various industries such as construction, car manufacturing industries, etc. (Megson (2012)). Depending on the geometry, loading conditions and also edge supports different studies are carried out to investigate the behavior of plates. When plates are subjected to compressive in-plane forces, they become unstable and buckle (Åkesson (2007), Chen *et al*. (2009)). Previous studies showed that plates' boundary conditions exert linearly and uniform distribute in-plane compressive (Chen (1976), Taylor (1933), Wang (1993), Musa (2016)).

Abolghasemi *et al*. (2015) investigated buckling of rectangular plates under non-uniform in-plane loading. Equilibrium equations were extracted based on the first order shear deformation theory. They studied buckling of plates under four types of in-plane loading, including the uniform, parabolic, cosine and triangular loadings and considered simply support boundary condition along the all edges. They investigated the effects of thickness and plate aspect ratio on the buckling load. Chang *et al*. (2004) presented exact solutions for the free vibration and buckling of rectangular plates with two edges clamped and the other two edges simply supported. It was assumed that in-plane stresses vary linearly. Buckling analysis of hybrid laminates under in-plane loads and different boundary conditions was presented by Belkacem *et al*. (2018). They used higher order shear and normal deformable theory of plate which is close to the three dimensional elasticity solution.

Engineering structures made of different materials such as Composites and FGMs are extensively used by researchers (Leissa (1987), Kapania and Raciti (1989), Turvey and Marshall (2012), Javaheri and Eslami (2002)). Reddy *et al*. (1989) presented exact analytical and numerical finite-element solutions for free vibration and buckling of laminated composite plates. The study was based on the classical, first-order and third-order plate theories and various boundary conditions are considered. They investigated the effects of material orthotropy, aspect ratio and side-to-thickness ratio on critical buckling loads. Thermal buckling behavior of composite laminated plates based on the classical theory and finite element method was shown by Shiau *et al*. (2010). They concluded that the thermal buckling mode depends on the aspect ratio. Javaheri *et al*. (2002) investigated thermal buckling of rectangular FGM plate based on the classical theory, where four types of thermal loading including uniform, linear and nonlinear temperature rise through the thickness, and also linear temperature changes through the length were studied. In addition, simply supported boundary conditions were supposed along the all edges. They concluded that increasing the aspect ratio increases the critical buckling temperature.

Lanhe *et al*. (2004) studied thermal buckling of thick rectangular FG plates based on the first order shear deformation theory with simply supported boundary conditions. They supposed two types of thermal loads including uniform temperature rise and gradient through the thickness. It was shown that by increasing the aspect ratio of the plate or the thickness to span ratio , critical buckling temperature difference increases. Tupal *et al*. (2018) studied shear buckling analysis of rectangular plates resting on elastic foundation. They used classical laminates theory for deriving the stability equations and also, solved equations by Reiliegh-Ritz method.

In recent years, many researches were focused on the reinforced composites and FG plates used in engineering

*Corresponding author, Assistant Professor
E-mail: meisam.mohammadi@vru.ac.ir
[a] M.Sc. Student

ISSN: 1225-4568 (Print), 1598-6217 (Online)

structures that are reinforced with shape memory alloy fibers (Thompson and Loughlan (1997), Ostachowicz *et al*. (2000), Kumar and Singh (2009)), electro-rheological fluids, smart materials, piezoelectric materials, etc. Smart materials such as shape memory alloys response to environment effects by changing their behavior. Park *et al*. (2004) investigated vibration of thermally post-buckled composite plates embedded with shape memory alloy fibers with simply supported boundary conditions based on the first-order shear deformation plate theory and nonlinear finite element method. The thermal post-buckling deflection was obtained according to the Newton–Raphson method. By embedding SMA fibers, the thermal large deflection decreases and the critical temperature increases. Although by using SMA fibers, weight of plate grows up, but the thermal large deflection reduces.

According to effects of shape memory alloys on performance of structures, it is necessary to study the behavior of engineering structures made of SMA. Lee *et al*. (2000) studied buckling and post buckling behavior of laminated composite (Carbon/Epoxy) shells with embedded shape memory alloy (SMA) wires under axial compressive forces and thermal loading for the cases of two boundary conditions including clamped–clamped and simply supported–simply supported boundary conditions by using ABAQUS. Liang and Roger's model was utilized by them. They concluded that the critical buckling load increases when the SMA wires activate in the direction of in-plane loads and decreases as the SMA wires activated in the opposite direction to the buckling load. Kou *et al*. (2009) studied buckling behavior of rectangular shape memory alloy reinforced composite laminates under in-plane boundary loading with simply supported boundary conditions. They employed the classical plate theory and finite element method in their study. Their Results showed that the active strain energy tuning method is much better than the active property tuning method in improving the buckling performance of plates. Also, it was inferred that the increase of SMA fiber volume fraction and pre-strain may generate more recovery stress which increase the stiffness of SMA reinforced composite laminates. Therefore, the critical buckling load varies significantly. Ibrahim *et al*. (2011) presented a new nonlinear finite element model for analyzing nonlinear panel flutter and thermal buckling characteristics of SMA hybrid composite plate based on first-order shear-deformable plate theory under thermal and aerodynamic loading. They used Newton–Raphson method for determining the deflection induced by thermal buckling. It was inferred that critical buckling temperature and critical non-dimensional dynamic pressure increase while the postbuckling deflection reduces in SMA embedded plate. Burton *et al*. (2006) simulated crack propagation in a composite reinforced plate by shape memory alloy wires by using ABAQUS software based on the one-dimensional constitutive model. Zhu *et al*. (2014) simulated a plate made of shape memory alloy with different configurations of pore arrays by ABAQUS software on the basis of kinematic hardening theory and also Stebner–Brinson model at high localized stresses. Thermal post-buckling analysis of shape memory alloy hybrid composite (SMAHC) shell panels based on the layer-wise theory by finite element method was investigated by Roh *et al*. (2004). They used Brinson's model to investigate the behaviors of shape memory alloy (SMA) wire. The composite and SMAHC panel's boundary conditions were supposed to be simply supported along all edges. Results showed that embedding SMA wires in composites prevent unstable post-buckling behaviors while they are lighter than composite panels.

According to the past researches, SMAs have great efficient on performance improvement of engineering structures. As the above literatures study reveals, there is no study on the buckling of SMA plates to investigate the stability of SMA plate. In the present article, buckling analysis of plates made of shape memory alloys under linearly and uniform distributed compressive in-plane forces is investigated. Kirchhoff plate theory is used for thin plate. Also, material properties are modeled based on Brinson's model. Finally the effects of loading conditions, boundary conditions, temperature and dimensions on the critical buckling loads are investigated in detail.

2. Material and constitutive model

Shape memory alloys are a new group of smart materials with special characteristics in thermal environment. Variation in SMA properties is due to solid phase transformation and molecular rearrangement. Two-phases are formed in the shape memory alloys including martensite and austenite phases. Martensite phase deforms easily and the molecular structure is twin in this phase. This phase is formed at low temperatures. Austenite phase is harder and firmer in comparison with martensite that forms at high temperature. Martensite phase deformation starts and finishes at temperatures M_s, M_f while the same temperature for austenite phase are defined as A_s and A_f. Shape memory alloys have two unique characteristics including shape memory effect and super elastic property. Different models were proposed for modeling the properties of SMAs. Brinson developed the model of Liang and Tanaka and suggested a new model for predicting the thermodynamic behavior of SMAs. Brinson's model is able to provide both shape memory effect and super elastic property by separating the volume fraction of martensite (ξ) into two parts: Stress-induced martensite (non-twinned martensite: ξ_S) and temperature-induced martensite (twinned martensite: ξ_T). This division is for justification of the micromechanical behavior of shape memory alloys. Hence, the proposed relation for volume fraction of martensite considering temperature and stress is stated as (Brinson (1993))

$$\xi = \xi_S + \xi_T \tag{1}$$

On the basis of Brinson's model (Brinson (1993)), the constitutive equation of SMAs can be expressed as

$$\sigma - \sigma_0 = E(\xi)(\varepsilon - \varepsilon_L \xi_S) + \alpha \Delta T \tag{2}$$

where σ is stress, σ_0 is initial stress, ε is strain, ξ is the internal variable representing the stage of the

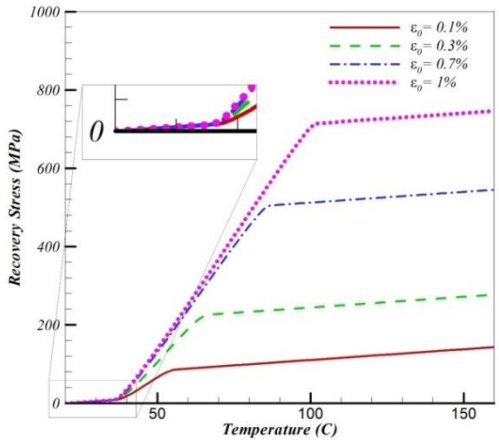

Fig. 1. Recovery stress versus temperature for SMA plate

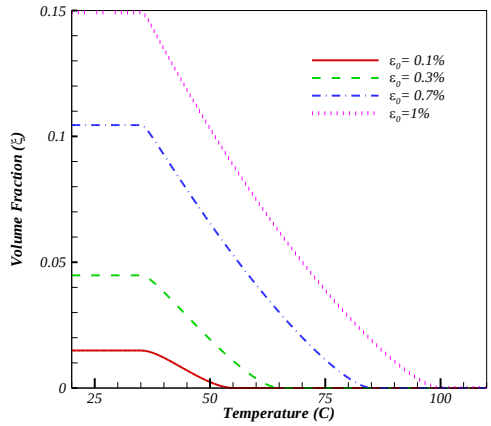

Fig. 2. The dependence of martensite fraction on temperature

transformation, ε_L is the maximum residual strain (obtained experimentally by converting to detwinned martensite and the unloading at a temperature less than the austenite start temperature), α is thermal expansion coefficient of the SMA material and T is the temperature. In addition, Young module of SMA plate is expressed as (Auricchio and Sacco (1997))

$$E(\xi) = \frac{E_A}{1 + (\frac{E_A}{E_M} - 1)\xi} \tag{3}$$

in which E_A and E_M are the Young moduli of SMA in the pure austenite and the pure martensite phases, respectively. Two relations to determine the martensite volume fractions during heating stage for $T > A_s$ and $C_A(T - A_f) < \sigma < C_A(T - A_s)$ state are (Brinson (1993))

$$\xi = \frac{(\xi_0)}{2}\left\{\cos\left[\frac{\pi}{A_f - A_s}\left(T - A_s - \frac{\sigma}{C_A}\right)\right] + 1\right\}$$

$$\xi_S = \xi_{S0} - \frac{\xi_{S0}}{\xi_0}(\xi_0 - \xi) \tag{4}$$

$$\xi_T = \xi_{T0} - \frac{\xi_{T0}}{\xi_0}(\xi_0 - \xi)$$

where the subscript $'0'$ demonstrates initial condition and the constants C_A is the slopes of the critical stress-temperature diagram for the austenite to martensite transformation and the reverse transformation, respectively.

Table 1 Thermomechanical properties of NiTi plate

Modulus (GPa)	Transformation temperature	Transformation constant	Material properties
$E_A = 67$	$M_f = 9^\circ C$	$C_M = 8(\frac{MPa}{^\circ C})$	$\varepsilon_L = 0.06$
	$M_s = 18.4^\circ C$	$C_A = 13.8(\frac{MPa}{^\circ C})$	$\alpha_A = 22\times10^{-6}(\frac{1}{^\circ C})$
$E_m = 26.3$	$A_s = 34.5^\circ C$	$\sigma_0 = 0$	$\alpha_M = 10\times10^{-6}(\frac{1}{^\circ C})$
	$A_f = 49^\circ C$	$\xi_{T0} = 0$	$\nu = 0.33$

In Fig. 1, variation of recovery stress with respect to the change of the temperature for Nitinol SMA is plotted for various pre-strains based on the Brinson's model. The transformation to austenite is the reason of large internal stresses. The effect of temperature on the SMA martensite volume fraction is depicted in Fig. 2. In this study, initial conditions and properties for rectangular plate made of SMA is presented in Table 1 (Asadi (2015)).

3. Formulation, analysis and solution method

3.1 Classical plate theory and energy method

Since it is assumed that SMA plate is thin, thus the classical plate theory (Kirchhoff plate theory) is used. According to this theory, components of displacement field are defined as

$$\begin{aligned} U(x,y,z) &= u_0(x,y) - z w(x,y)_{,x} \\ V(x,y,z) &= v_0(x,y) - z w(x,y)_{,y} \\ W(x,y,z) &= w(x,y) \end{aligned} \tag{5}$$

In Eq. (5), $U(x,y,z)$, v and w are the components of the displacement field in x, y and z directions respectively. Also, u_0 and v_0 are the in-plane components of displacement field and w is the transverse displacement of the mid-plane in z direction. In addition, $w_{,x}$ and $w_{,y}$ indicate the first derivative of plate deflection with respect to the x, y variables, respectively. Strain components of SMA plate considering the Von-Karman hypothesis are simplified as

$$\begin{aligned} \varepsilon_x &= \frac{\partial u}{\partial x} + \frac{1}{2}(\frac{\partial w}{\partial x})^2 \\ \varepsilon_y &= \frac{\partial v}{\partial y} + \frac{1}{2}(\frac{\partial w}{\partial y})^2 \\ \gamma_{xy} &= \frac{\partial u}{\partial y} + \frac{\partial v}{\partial x} + \frac{\partial w}{\partial x}\frac{\partial w}{\partial y} \end{aligned} \tag{6}$$

Variational approach and principle of minimum total potential energy is used for deriving the components of Eq. (6). Accordingly, the variation of total energy of SMA plate is defined as (Ventsel and Krauthammer (2001)).

$$\Delta\Pi = \Pi - \Pi_0 = \Delta U_0 + U_b + \Delta\Omega_r \quad (7)$$

where ΔU_0 is the increment of the strain energy of the plate , U_b is the strain energy of bending and twisting and $\Delta\Omega_r$ is the increment in the potential energy of in-plane external edge forces applied to the plate edges. The strain energy stored in an elastic body considering plane stress state is given by

$$\Delta U_0 = \frac{1}{2}\iiint_V \left(\sigma_x \varepsilon_x + \sigma_y \varepsilon_y + \tau_{xy}\gamma_{xy}\right)dV \quad (8)$$

Equation (8) is simplified using the following expression

$$\sigma_x = \frac{\hat{N}_x}{h}$$
$$\sigma_y = \frac{\hat{N}_y}{h} \quad (9)$$
$$\tau_{xy} = \frac{\hat{N}_{xy}}{h}$$

where $\hat{N}_x$, $\hat{N}_y$, and $\hat{N}_{xy}$ are resultant forces in x, y and xy directions, respectively. Substituting the above equation and Eq. (6) into Eq. (8) and integrating over the plate thickness, results in the following expression for the increment in the strain energy of plates' middle surface is expressed as

$$\Delta U_0 = \iint_A [\hat{N}_x\frac{\partial u}{\partial x} + \hat{N}_y\frac{\partial v}{\partial y} + \hat{N}_{xy}\left(\frac{\partial u}{\partial y} + \frac{\partial v}{\partial x}\right)dxdy + \frac{1}{2}\iint_A [\hat{N}_x(\frac{\partial w}{\partial x})^2 + \hat{N}_y\left(\frac{\partial w}{\partial y}\right)^2 + 2\,\hat{N}_{xy}\left(\frac{\partial w}{\partial y}\frac{\partial w}{\partial x}\right)\Big]dxdy \quad (10)$$

The first integral on the right-hand side of Eq. (10) represent the work, W_e done by the in-plane external forces applied to the middle surface of plate. Thus, the expression (10) is written as

$$\Delta U_0 = W_e + \frac{1}{2}\iint_A [\widehat{N_x}(\frac{\partial w}{\partial x})^2 + \widehat{N_y}\left(\frac{\partial w}{\partial y}\right)^2 + 2\,\widehat{N_{xy}}\left(\frac{\partial w}{\partial y}\frac{\partial w}{\partial x}\right)\Big]dxdy \quad (11)$$

It can be shown that the expression for ΔU_0 in the form of Eq. (11) is valid for plates of any geometry, not necessarily, rectangular. The increment in the potential of the external, in-plane forces applied to the plate is equal to the negative work done by these forces, i.e.

$$\Delta\Omega_r = -W_e \quad (12)$$

By introducing the generalized Hooke's law for isotropic materials, Eq. (8) for strain energy is reduced to the following form as

$$U_b = \iiint_V [\frac{1}{2E}(\sigma_x{}^2 + \sigma_y{}^2 - 2\nu\sigma_x\sigma_y) + \frac{1+\nu}{E}\tau_{xy}{}^2]dV \quad (13)$$

By substituting Eq. (6) and Hooke's law into Eq. (13) and integrating over the thickness of plate, strain energy of deformation is expressed as

$$U_b = \frac{1}{2}\iint_A D\{(\frac{\partial^2 w}{\partial x^2} + \frac{\partial^2 w}{\partial y^2})^2 - 2(1-\nu)[\frac{\partial^2 w}{\partial x^2}\frac{\partial^2 w}{\partial y^2} - (\frac{\partial^2 w}{\partial x\,\partial y})^2]\} \quad (14)$$

Where D is flexural rigidity of plate that is defined so that

$$D = \frac{Eh^3}{12(1-\nu^2)} \quad (15)$$

Therefore, the increment in the total potential energy of the plate upon buckling according to Eq. (7) is written in the following form

$$\Delta\Pi = \frac{1}{2}\iint_A D\{(\frac{\partial^2 w}{\partial x^2} + \frac{\partial^2 w}{\partial y^2})^2 + 2(1-\nu)[\frac{\partial^2 w}{\partial x\,\partial y})^2 - \frac{\partial^2 w}{\partial x^2}\frac{\partial^2 w}{\partial y^2}]\}dxdy + \frac{1}{2}\iint_A [\hat{N}_x(\frac{\partial w}{\partial x})^2 + \hat{N}_y(\frac{\partial w}{\partial y})^2 + 2\,\hat{N}_{xy}\frac{\partial w}{\partial x}\frac{\partial w}{\partial y}]dxdy \quad (16)$$

where $\hat{N}$ is the resultant force in the middle surface of SMA plate due to the applied in-plane loads that is expressed as

$$\hat{N} = N^0 + N^r - N^T \quad (17)$$

In the above equation, N^0 is the stress resultant due to the mechanical external loads, N^r is the resultant force induced by recovery stress and N^T is the thermal resultant force which are obtained from Eq. (18) as (Mahabadi *et al*. (2016))

$$\begin{bmatrix} N_x^T \\ N_y^T \\ N_{xy}^T \end{bmatrix} = \int_{-\frac{h}{2}}^{\frac{h}{2}} \begin{bmatrix} \frac{E(\xi)}{1-\nu^2} & \frac{E(\xi)\nu}{1-\nu^2} & 0 \\ \frac{E(\xi)\nu}{1-\nu^2} & \frac{E(\xi)}{1-\nu^2} & 0 \\ 0 & 0 & \frac{E(\xi)}{2(1+\nu)} \end{bmatrix} \times \begin{bmatrix} \alpha \\ \alpha \\ 0 \end{bmatrix} \Delta T dz$$
$$\begin{bmatrix} N_x^r \\ N_y^r \\ N_{xy}^r \end{bmatrix} = \int_{-\frac{h}{2}}^{\frac{h}{2}} \sigma^r \times \begin{bmatrix} \alpha \\ \alpha \\ 0 \end{bmatrix} \Delta T dz \quad (18)$$

Bifurcation of an initial configuration of equilibrium occurs when

$$\Delta\Pi = 0 \quad (19)$$

This is the general energy criterion for the buckling analysis of plates. The latter can also be employed for constructing an approximate solution of the plate buckling

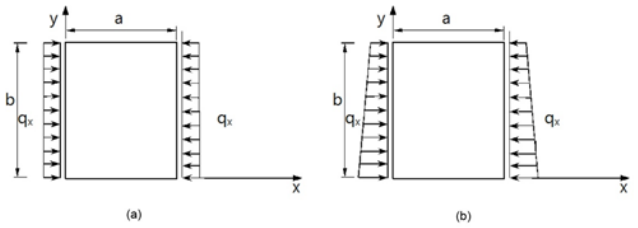

Fig. 3 Loading condition on SMA plate: (a) uniform (b) linearly

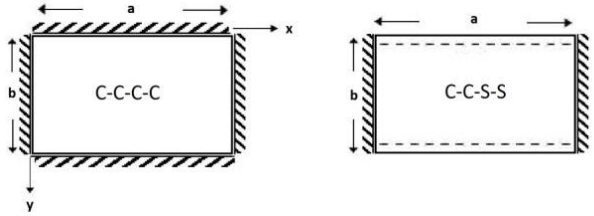

Fig. 4 Boundary condition of SMA plate

Table 2 Algebraic polynomials for typical boundary conditions

Boundary conditions	$X_i(x)$	$Y_j(y)$
S-S-S-S	$(\frac{x}{a})^{i+1}-2(\frac{x}{a})^{i+2}+(\frac{x}{a})^{i+3}$	$\left(\frac{y}{b}\right)^{j+1}-2\left(\frac{y}{b}\right)^{j+2}+\left(\frac{y}{b}\right)^{j+3}$
C-C-C-C	$(\frac{x}{a})^{i+1}-2(\frac{x}{a})^{i+2}+(\frac{x}{a})^{i+3}$	$(\frac{y}{b})^{j+1}-2(\frac{y}{b})^{j+2}+(\frac{y}{b})^{j+3}$
C-C-S-S	$(\frac{x}{a})^{i+1}-2(\frac{x}{a})^{i+2}+(\frac{x}{a})^{i+3}$	$(\frac{y}{b})^{j}-(\frac{y}{b})^{j+1}$

problems. In the following, the critical buckling load of SMA rectangular plate will be determined under linearly and uniformly distributed compressive in-plane forces and various boundary conditions by using Ritz method.

3.2 Loading and boundary conditions

The plate is loaded by linearly distributed compressive in-plane forces with equation $q_x = -q(1+\eta\frac{y}{b})$ along the plate width (See Fig. 3). By setting 0 for η the SMA plate is loaded uniformly and if $\eta = 1$, the SMA plate is subjected to linearly distributed loads.

Also, various boundary conditions may be considered for rectangular SMA plate. Hence, as shown in Figure 4, two cases of boundary conditions are assumed in the present study.

3.3 Ritz method

In this paper, Ritz method is used for solving the stability equations for buckling analysis of rectangular plate made of SMA with various boundary conditions. According to the Ritz method, the deflection surface of plate considering the boundary conditions is approximated as (Reddy (2017))

$$w(x,y) = \sum_{j=1}^{n}\sum_{i=1}^{m} w_{ij} X_i(x) Y_j(y) \qquad (20)$$

Table 3 Comparing the critical buckling load (N / m) for SMA simply supported plate subjected to uniform loading based on the Ritz and Navier methods

a/b	Ritz method	Navier method
0.5	165.2	167.3
1	103.	103.4
1.5	81.1	82.0

Table 4 The convergence study of the Ritz method for critical buckling load of SMA plate subjected to uniform load

i, j	$a/b = 0.5$	$a/b = 1$	$a/b = 1.5$
(1,1)	165.2	110.2	240.7
(1,2)	165.3	103.0	81.1
(1,3)	165.1	102.9	81.1
(2,2)	165.2	103.0	81.1

It is clear that accuracy of solution depends on the number of terms in series presented in Eq. (20). In the following, the first two terms are considered. One of the choices for the functions X_i and Y_j are algebraic polynomials. For the assumed boundary condition consist of S-S-S-S, C-C-C-C and C-C-S-S , these functions are given in Table 2 (Reddy (2017)).

3.4 Validation

In order to validate the presented study, an exact solution is obtained for simply supported plate based on the Navier solution (Ventsel and Krauthammer (2001)). According to the Navier solution which is an exact and closed form solution, critical buckling load for S-S-S-S plate is determined as

$$\frac{D}{a^4b^4}\left(\begin{matrix}D\pi^2a^4n^2+2D\pi^2a^2b^2m^2n^2\\+D\pi^2b^4m^4+N_xa^2b^4m^2+N_ya^4b^2n^2\end{matrix}\right)=0 \qquad (21)$$

In Table 3, a comparison is presented for the critical buckling loads based on the Navier and Ritz methods for simply supported plates in room temperature subjected to uniform load.

According to the table, there is a good agreement between the presented results based on the Ritz method and Navier method.

Since Ritz method is used for determining the results, convergence study is done on the solution. Hence, in Table 4, numerical results for simply supported SMA plate subjected to uniformly distributed load in room temperature is tabulated($T = 25\ ℃$).

According to the presented results in Table 4, in the following two terms are considered for i and j.

4. Results and discussion

According to Fig. 3, pre-buckling forces are determined as $N_x^0 = q_x$ and $N_y^0 = N_{xy}^0 = 0$. Using equations (16), (19)

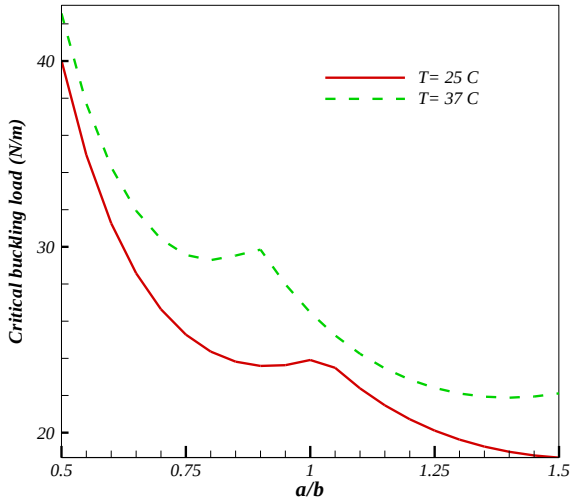

Fig. 5 The critical buckling load for a C-C-C-C plate versus the aspect ratio under uniform loading

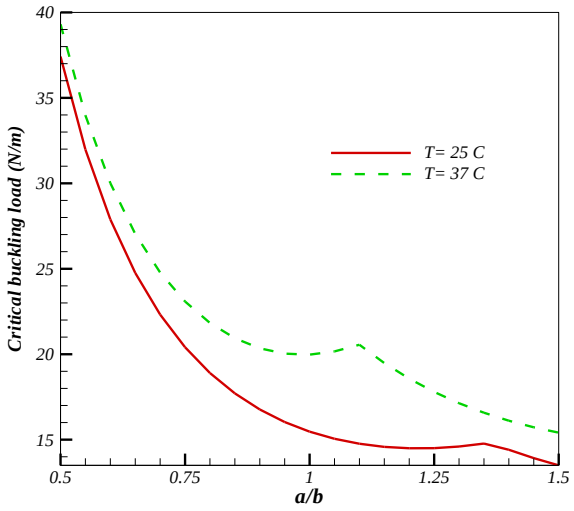

Fig. 6 The critical buckling load for a C-C-S-S plate versus the aspect ratio under uniform loading

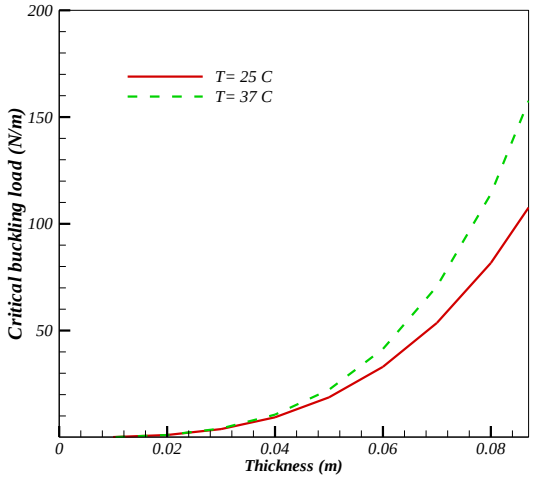

Fig. 7. The critical buckling load for a C-C-C-C plate versus the thickness at ($\frac{a}{b} = 1.5$) under uniform loading

Table 5 Critical buckling load (N) for SMA plate subjected to uniform loading

Temperature	a/b	C-C-C-C	C-C-S-S
$T = 25^{\circ}C$	0.5	40.0	37.4
	1	23.9	15.5
	1.5	18.7	13.5
$T = 37^{\circ}C$	0.5	42.5	39.3
	1	26.5	20.0
	1.5	22.1	15.4

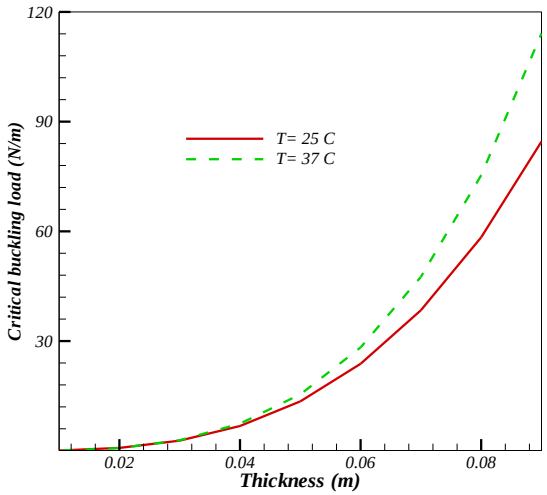

Fig. 8. The critical buckling load for a C-C-S-S plate versus the thickness at ($\frac{a}{b} = 1.5$) under uniform loading

and (20), the critical buckling loads are determined. It should be noted that N^r and N^T are the same as pre-stresses due to recovery stress and thermal loads. Also, for determining the flexural rigidity of SMA plate, Young modulus of SMA plate must be calculated for each temperature and martensite volume fraction (ξ) based on Fig. 2.

4.1 Uniform compressive in-plane forces

Consider a rectangular SMA plate with thickness 0.05 m which is subjected to uniform compressive load (η=0) so that $q_x = -q$. In tables 5 and 6, critical buckling loads for different aspect ratios, thickness to side ratios and various temperatures are tabulated.

In figures 5 and 6, the effect of aspect ratio and temperature on the critical buckling load is shown. According to these figures, increasing the aspect ratio usually decreases the critical buckling load. Also, the critical buckling mode may change as the aspect ratio increases. As figures show, increasing the temperature from the room temperature (T = 25 ℃) to body temperature (T = 37 ℃), leads to increasing the critical buckling load.

The effect of thickness on the critical buckling load of SMA plate for different boundary conditions and various temperatures are depicted in figures 7 and 8. According to these figures, increasing the thickness of SMA plate

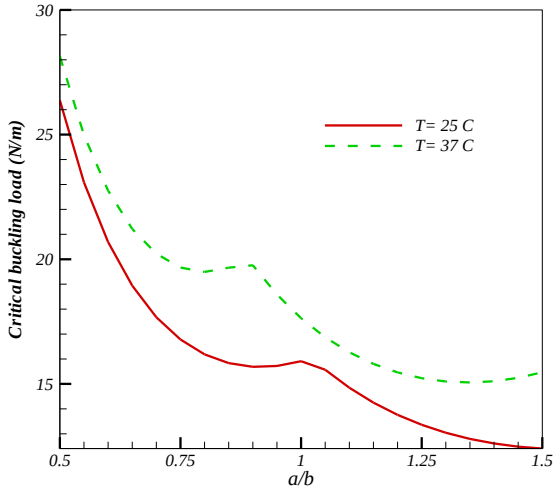

Fig. 9 The critical buckling load for a C-C-C-C plate versus the aspect ratio under linearly loading

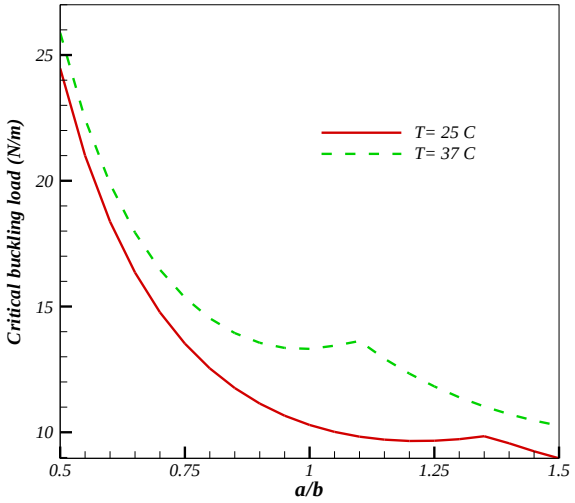

Fig. 10 The critical buckling load for a C-C-S-S plate versus the aspect ratio under linearly loading

Table 6 The effect of thickness on the critical buckling load of SMA plate under uniform loading (a/b =1.5)

Thickness (m)	C-C-C-C		C-C-S-S	
	$T = 25^{\circ}C$	$T = 37^{\circ}C$	$T = 25^{\circ}C$	$T = 37^{\circ}C$
0.01	0.1	0.1	0.01	0.02
0.02	1.1	1.1	0.8	0.7
0.03	3.8	4.1	2.8	2.9
0.04	9.4	10.6	6.8	7.4
0.05	18.7	22.3	13.5	15.4
0.06	33.0	41.4	23.8	28.2
0.07	53.6	70.7	38.4	47.6
0.08	81.6	114.0	58.4	75.3
0.09	18.7	176.3	84.5	114.1

increases the critical buckling load. Also, this variation is more apparent for thick plates.

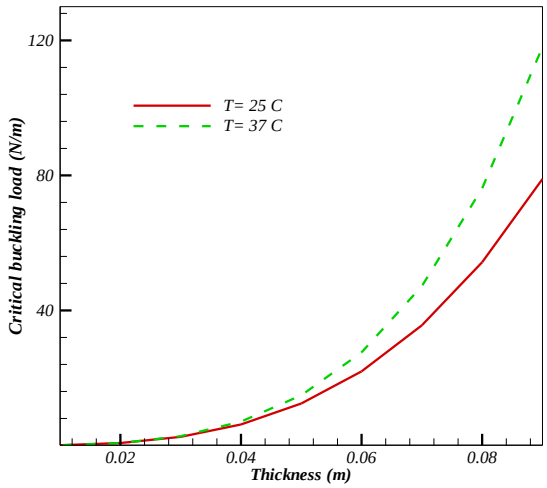

a) C-C-C-C plate

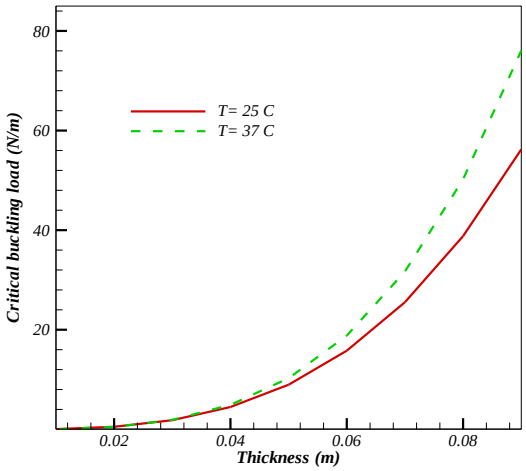

b) C-C-S-S plate

Fig. 11. The critical buckling load versus the thickness ($\frac{a}{b} = 1.5$) under linearly loading

4.2 Linearly distributed in-plane forces

In this case, it is assumed that SAM plate is subjected to linearly distributed loads by the function $q_x = -q\,(1 + \frac{y}{b})$. In tables 7 and 8, the effects of thickness, aspect ratio, temperature and boundary conditions on the critical buckling loads are presented.

In order to have a qualitative study, variation of critical buckling load versus the aspect ratio and thickness is depicted in figures 9 to 12. According to these figures, critical buckling mode changes as the temperature and aspect ratio change.

4.3 Special case: Triangular loading

In order to study different loading conditions, it is assumed that SMA simply supported plate is subjected to in-plane triangular distributed load. In Fig. 12 , the effect of aspect ratio on the critical buckling load is shown at room temperature ($T = 25\,^{\circ}C$). As shown in this figure, critical buckling load decreases by increasing the aspect ratio until $\frac{a}{b} = 1$. The

Table 7 Critical buckling load (N) for SMA plate subjected to linearly distributed loads

Temperature	a/b	C-C-C-C	C-C-S-S
$T=25^{\circ}C$	0.5	26.4	24.5
	1	15.9	10.3
	1.5	12.4	9.0
$T=37^{\circ}C$	0.5	28.1	25.9
	1	17.6	13.3
	1.5	15.5	10.3

Table 8 The effect of thickness on the critical buckling load of SMA plate under linearly distributed load ($a/b=1.5$)

Thickness (m)	C-C-C-C		C-C-S-S	
	$T=25^{\circ}C$	$T=37^{\circ}C$	$T=25^{\circ}C$	$T=37^{\circ}C$
0.01	0.07	0.05	0.05	0.02
0.02	0.7	0.7	0.5	0.5
0.03	2.5	2.7	1.8	1.9
0.04	6.2	7.1	4.5	4.9
0.05	12.4	14.8	9.0	10.3
0.06	21.	27.	15.8	18.8
0.07	35.6	47.2	25.5	31.7
0.08	54.3	76.2	38.8	50.2
0.09	79.0	118.0	56.2	76.1

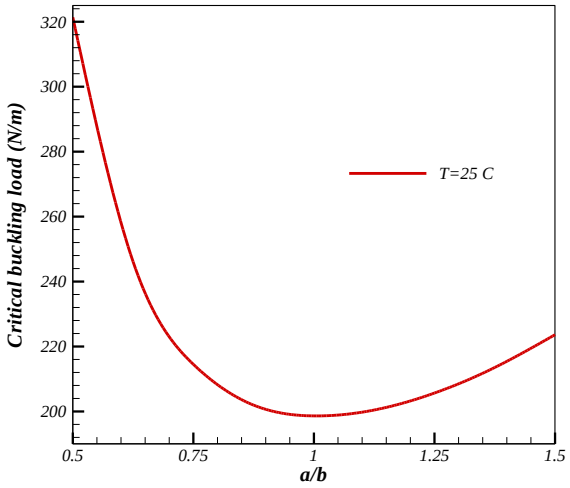

Fig. 12 Variation of critical buckling load for a S-S-S-S plate versus the aspect ratio under triangular loading

minimum buckling load is obtained for square SMA plate. Also, variation of critical buckling load is more apparent for SMA plate with aspect ratio less than 0.5.

5. Conclusion

In the present study, a semi-analytical solution was presented to investigate the buckling behavior of SMA plate. Brinson's model was used for predicting the behavior SMA plate. Critical buckling load was calculated based on classical theory plate where the SMA plate was subjected to uniform and linearly distributed loads. Two types of boundary conditions were considered for SMA plate at body and room temperatures.

According to the numerical results, increasing the aspect ratio may increase the critical buckling loads. Also, it was concluded that critical buckling mode may change as the aspect ratio, temperature or boundary condition changes. Based on the numerical results, it was concluded that as the boundary constraint changes to all clamped edges, critical buckling load increases in comparison with the other studied case.

References

Abolghasemi, S., Eipakchi, H. and Shariati, M. (2015), "Analytical solution for buckling of rectangular plates subjected to non-uniform in-plane loading based on first order shear deformation theory", *Modares Mech. Eng.*, **14**.

Åkesson, B. (2007), *Plate Buckling in Bridges and Other Structures*, *CRC Press*, U.S.A.

Asadi, H., Akbarzadeh, A., Chen, Z. and Aghdam, M. (2015), "Enhanced thermal stability of functionally graded sandwich cylindrical shells by shape memory alloys", *Smart Mater. Struct.*, **24**. 045022.

Auricchio, F. and Sacco, E. (1997), "A one-dimensional model for superelastic shape-memory alloys with different elastic properties between austenite and martensite", *J. Non-Linear Mech.*, **32**(6), 1101-1114, https://doi.org/10.1016/S0020-7462(96)00130-8.

Belkacem, A., Tahar, H.D., Abderrezak, R., Amine, B.M., Mohamed Z. and Boussad, A. (2018), "Mechanical buckling analysis of hybrid laminated composite plates under different boundary conditions" *Struct. Eng. Mech.*, **66**. https://doi.org/10.12989/sem.2018.66.6.761.

Brinson, L.C. (1993), "One-dimensional constitutive behavior of shape memory alloys: thermomechanical derivation with non-constant material functions and redefined martensite internal variable", *J. Int. Mater. Syst. Struct.*, **4**, 229-242. https://doi.org/10.1177/1045389X9300400213.

Burton, D., Gao, X. and Brinson, L. (2006), "Finite element simulation of a self-healing shape memory alloy composite", *Mech. Mater.*, **38**, 525-537. https://doi.org/10.1016/j.mechmat.2005.05.021.

Chang, K.H., Shim, H.J. and Kang, J.H. (2004), "Free vibrations and buckling of rectangular plates with linearly varying in-plane loading", *J. Korean Assoc. Spatial Struct.*, **4,** 99-111.

Chen, T.L. (1967), "Design of composite-material plates for maximum uniaxial compressive buckling load", *Proceedings of the Oklahoma Academy of Science*, 104-107.

Chen, Y., Lee, Y., Li, Q. and Guo, Y. (2009), "Concise formula for the critical buckling stresses of an elastic plate under biaxial compression and shear", *J. Construct. Steel Res.*, **65**, 1507-1510. https://doi.org/10.1016/j.jcsr.2009.02.006.

Ibrahim, H.H., Tawfik, M. and Negm, H.M. (2011), "Thermal buckling and nonlinear flutter behavior of shape memory alloy hybrid composite plates", *J. Vib. Control*, **17,** 321-333. https://doi.org/10.1177/1077546309353368.

Javaheri, R. and Eslami, M. (2002), "Buckling of Functionally Graded Plates under In plane Compressive Loading", *Journal of Applied Mathematics and Mechanics/Zeitschrift für Angewandte Mathematik und Mechanik*, **82**, 277-283.

Javaheri, R. and Eslami, M. (2002), "Thermal buckling of functionally graded plates", *AIAA J.*, **40**, 162-184. https://doi.org/10.2514/2.1626.

Kapania, R.K. and Raciti, S. (1989), "Recent advances in analysis of laminated beams and plates, Part I: Shear effects and buckling", *AIAA J.,* **27**, 923-935. https://doi.org/10.2514/3.10202.

Kumar, S. and Singh, B. (2009), "Thermal buckling analysis of SMA fiber-reinforced composite plates using layerwise model", *J. Aerosp. Eng.*, **22**, 342-353.

Kuo, S.Y., Shiau, L.C. and Chen, K.H. (2009), "Buckling analysis of shape memory alloy reinforced composite laminates", *Compos. Struct.*, **90**, 188-195. https://doi.org/10.1016/j.compstruct.2009.03.007.

Lanhe, W. (2004), "Thermal buckling of a simply supported moderately thick rectangular FGM plate" *Compos. Struct.*, **64**, 211-218. https://doi.org/10.1016/j.compstruct.2003.08.004.

Lee, H.J. and Lee, J.J. (2000), "A numerical analysis of the buckling and postbuckling behavior of laminated composite shells with embedded shape memory alloy wire actuators", *Smart Mater. Struct.*, **9,** 780-790.

Leissa, A.W. (1987), "A review of laminated composite plate buckling", *Appl. Mech. Rev.* **40**, 575-591. http://doi.org/10.1115/1.3149534. https://doi.org/10.1115/1.3149534.

Mahabadi, R.K., Shakeri, M. and Pazhooh, M.D. (2016), "Free vibration of laminated composite plate with shape memory alloy fibers", *Latin American J. Solids Struct.,* **13**, 314-330. http://dx.doi.org/10.1590/1679-78252162.

Megson, T.H.G. (2012), *Aircraft Struct. Eng. Students*, Butterworth-Heinemann, Oxford, United Kingdom.

Musa, I.A. (2016), "Buckling of plates including effect of shear deformations: A hyperelastic formulation", *Struct. Eng. Mech.,* **57**.

Ostachowicz, W., Krawczuk, M. and Żak, A. (2000), "Dynamics and buckling of a multilayer composite plate with embedded SMA wires", *Compos. Struct.,* **48**, 163-167. https://doi.org/10.1016/S0263-8223(99)00090-2.

Park, J.S., Kim, J.H. and Moon, S.H. (2004), "Vibration of thermally post-buckled composite plates embedded with shape memory alloy fibers", *Compos. Struct.*, **63**, 179-188. https://doi.org/10.1016/S0263-8223(03)00146-6.

Reddy, J. and Khdeir, A. (1989), "Buckling and vibration of laminated composite plates using various plate theories" *AIAA J.*, **27**, 1808-1817. https://doi.org/10.2514/3.10338.

Reddy, J.N. (2017), *Energy Principles and Variational Methods in Applied Mechanics*, John Wiley & Sons, U.S.A.

Roh, J.H., Oh, I.K., Yang, S.M., Han, J.H. and Lee, I. (2004), "Thermal post-buckling analysis of shape memory alloy hybrid composite shell panels", *Smart Mater. Struct.*, **13**, 1337.

Shiau, L.C., Kuo, S.Y. and Chen, C.Y. (2010), "Thermal buckling behavior of composite laminated plates", *Compos. Struct.*, **92**, 508-514. https://doi.org/10.1016/j.compstruct.2009.08.035.

Taylor, G. (1933), "The buckling load for a rectangular plate with four clamped edges", *ZAMM Journal of Applied Mathematics and Mechanics/Zeitschrift für Angewandte Mathematik und Mechanik,* **13,** 147-152.

Thompson, S. and Loughlan, J. (1997), "Adaptive post-buckling response of carbon fibre composite plates employing SMA actuators", *Compos. Struct.*, **38**, 667-678. https://doi.org/10.1016/S0263-8223(97)00104-9.

Tupal, U., Nazarimofrad E. and Sadat Kholerdi S.E. (2018), "Shear buckling analysis of cross-ply laminated plates resting on Pasternak foundation", *Struct. Eng. Mech.,* **68**.

Turvey, G.J. and Marshall, I.H. (2012), *Buckling and Postbuckling of Composite Plates*, Springer Science & Business Media, Germany.

Ventsel, E. and Krauthammer, T. (2001), *Thin Plates and Shells: Theory: Analysis, and Applications*, CRC Press, USA.

Wang, X., Bert, C. and Striz, A. (1993), "Differential quadrature analysis of deflection, buckling, and free vibration of beams and rectangular plates", *Comput. Struct.*, **48**, 473-479. https://doi.org/10.1016/0045-7949(93)90324-7.

Zhu, P., Stebner, A.P. and Brinson, L.C. (2014), "Plastic and transformation interactions of pores in shape memory alloy plates", *Smart Mater. Struct.*, **23**, 104008.

CC